Available online at www.sciencedirect.com

ScienceDirect

Applied Mathematical Modelling 32 (2008) 12–27

APPLIED MATHEMATICAL MODELLING

www.elsevier.com/locate/apm

Modeling analysis of the electromagnetic braking action on rotating solid cylinders

Oriano Bottauscio [a,*], Mario Chiampi [b], Alessandra Manzin [a]

[a] *Istituto Nazionale di Ricerca Metrologica (I.N.RI.M.), Strada delle Cacce 91, 10135 Torino, Italy*

[b] *Politecnico di Torino, Dipartimento di Ingegneria Elettrica, Corso Duca degli Abruzzi 24, I-10129 Torino, Italy*

Received 1 January 2006; received in revised form 1 October 2006; accepted 24 October 2006
Available online 18 December 2006

Abstract

The electromagnetic diffusion and the electromechanical phenomena arising in a solid cylinder rotating inside a magnetic field are here analyzed. The study is developed through a time stepping Finite Element voltage-driven formulation, employing the sliding mesh technique for handling the cylinder motion. The influence on the dynamic behavior and energy dissipation of the material electric and magnetic properties, the geometrical parameters and the supply conditions is investigated considering a model problem.

Keywords: Moving systems; Eddy currents; Non-linear media; Magneto-mechanical coupled problems; Finite element sliding mesh

1. Introduction

One of the most important areas of interest in the power engineering involves the computation of the induced electric field and the associated eddy currents in rotating structures. In fact, when an electrical conductor rotates in a magnetic field, currents are induced within the material [1]. These eddy currents, which tend to cancel the magnetic field inside the conductor, give rise to electromagnetic forces and to energy transformation into the form of heat. The first phenomenon determines the device mechanical behavior; the second one produces an undesirable increment of the rotor temperature. The prediction of these coupled phenomena is essential in the analysis of the magnetic bearing and brake actuators, as well as more generally in the study of the electrical machines [2–8].

The aim of the present paper, focused on the braking action, is the modeling analysis of the electromagnetic phenomena arising when a solid structure rotates inside a magnetic field. The attention is intentionally addressed to a two-dimensional problem, where a solid cylinder is rotating between the poles of an electromagnet supplied by a known voltage generator. In this model problem, the cylinder is initially supposed to

* Corresponding author. Tel.: +39 (0) 11 3919828; fax: +39 (0) 11 3919849.
E-mail addresses: botta@inrim.it (O. Bottauscio), mario.chiampi@polito.it (M. Chiampi), manzin@inrim.it (A. Manzin).

0307-904X/$ - see front matter
doi:10.1016/j.apm.2006.10.021

rotate at a given angular speed, friction-less and without a driving torque; after the current making in the supply circuit, the induced phenomena in the conductive solid cylinder give rise to a braking action, which causes a gradual reduction of the rotor angular speed. The electromagnetic diffusion phenomena inside the cylinder are strongly dependent on the material properties and their evolution during the transient state affects, in a very complex way, the electromechanical behavior and the energy dissipation mechanism. Despite the simple geometry and the two-dimensional approximation, which are not representative of an actual device, all the electromagnetic and electromechanical phenomena arising in the considered structure are taken into account, allowing us to deeply investigate the influence on the braking action of the material properties, the geometrical parameters and the supply conditions.

The modeling analysis of the considered problem requires the coupling of several physical phenomena, which can be so synthesized: (i) arising of eddy currents in solid conductive materials, directly responsible for the braking torque, (ii) non-linear and hysteretic behavior of magnetic materials, producing local saturations and time delays, (iii) interaction between electromagnetic field and electric supply circuits, (iv) mechanical effect on the rotating parts, and finally (v) energy dissipation mechanisms. The simulation of all these phenomena is not usual in the commercial tools, so that a specific mathematical engine has been developed. The approach is based on a two-dimensional Finite element (FE) solution of the Maxwell's equations, handling the magnetic non-linearities and the hysteresis by the Fixed Point iterative technique and modeling the cylinder rotation through the sliding mesh technique [9–11]. The transient time evolution is treated by a step-by-step procedure.

A detailed description of the modeling approach is presented in Section 2. In Section 3 the numerical procedure is applied to the analysis of pure conductive and ferromagnetic rotating cylinders, investigating the physical phenomena arising in the rotor and discussing the influence of different parameters on the braking action.

2. Electromagneto-mechanical model

The behaviour of the considered device results from the combination of different physical phenomena:

- the eddy currents arising in non-linear and hysteretic materials;
- the electromagnetic interaction with the electric network;
- the mechanical torques acting on rotating components.

Therefore the modelling approach is based on three systems of equations, respectively describing the electromagnetic problem, including eddy current and hysteresis effects, the supply circuit behaviour and the mechanical laws. In particular, the analysis of the transient evolution is performed by a step-by-step time procedure: at each time instant, after the solution of the combined field-circuit problem, driven by a voltage source, and the consequent estimation of the electromagnetic torque, the rotor angular displacement is calculated by means of the mechanical equations. Then, the computed motion is imposed on the moving object, in order to update the domain configuration for the next instant.

2.1. Electromagnetic field problem

In this paper the FE formulation is developed for a two-dimensional problem, assuming geometric and physical properties invariant along one of the coordinate axis. Considering a Cartesian coordinate system, the magnetic flux density vector $\boldsymbol{b}$ is supposed to lay in the (x,y) plane and to be independent from coordinate z, while the currents flow along z-axis. Then, omitting the time dependency, vector quantities $\boldsymbol{b}$ and current density $\boldsymbol{j}$ result defined as

$$\boldsymbol{b} = (b_x(x,y), b_y(x,y), 0),$$
$$\boldsymbol{j} = (0, 0, j_z(x,y)).$$

Expressing field vector $\boldsymbol{b}$ as the curl of a vector potential $\boldsymbol{a} = (0, 0, a(x, y))$, so that div$\boldsymbol{a} = 0$, and considering the magnetic constitutive relationship $\boldsymbol{h} = \zeta(\boldsymbol{b})$ between magnetic field $\boldsymbol{h}$ and magnetic flux density $\boldsymbol{b}$, the following electromagnetic field equation is obtained:

$$\mathrm{curl}[\zeta(\mathrm{curl}\,\boldsymbol{a})] = \boldsymbol{j}. \tag{1}$$

In Eq. (1), which represents the starting point for the electromagnetic field analysis, the unknown quantity is the z-component of the magnetic vector potential. Vector $\boldsymbol{j}$ includes the presence of exciting windings and eddy currents in conductive materials (non-magnetic or ferromagnetic). Thus, two types of conductors are distinguished: the conductive regions having an electrical conductivity different from zero, indicated as *electromagnetic conductors*, and the *circuit conductors*, including the device components electrically connected to the supply circuit (e.g. the windings traces). In the first conductors the eddy current phenomena are taken into account, and then the solid cylinder is assumed as an *electromagnetic conductor*. The second category includes both bulk conductors (generally conductive rings or traces of coils having a few turns) and windings composed of numerous filaments. In the last case the current density distribution results uniform, because the conductor cross-sectional area is supposed to be too small to allow a local influence of eddy currents. In the studied problem, the supply windings are constituted of filamentary conductors, so that vector $\boldsymbol{j}$ results expressed as

$$j = -\sum_k \left[\sigma_k \dot{a} - \left(\frac{\sigma_k}{S_k}\int_{\Omega_k} \dot{a}\,\mathrm{d}s\right)\right] \Gamma_k \boldsymbol{u}_z + \sum_p \frac{N_p i_p}{S_p} \Gamma_p \boldsymbol{u}_z, \tag{2}$$

where $\boldsymbol{u}_z$ is the unit vector along z-direction. Index p indicates a winding composed of N_p filaments and carrying a current i_p (Fig. 1). In the present problem, where the source voltages are assigned (voltage driven problem), this current is unknown and depends both on the field distribution and on the supply circuit features. Index k indicates a generic *electromagnetic conductor*, having electrical conductivity σ_k and occupying a region of trace Ω_k and area S_k. The characteristic function Γ_k is defined as

$$\Gamma_k(x, y) = \begin{cases} 1 & \text{if} \quad (x, y) \in \Omega_k \\ 0 & \text{if} \quad (x, y) \notin \Omega_k. \end{cases}$$

The constitutive relationship $\boldsymbol{h} = \zeta(b)$ appearing in Eq. (1) takes into account the magnetic non-linearity, due to the presence of ferromagnetic materials, which exhibit saturation effects. The method here employed for treating non-linear problems is the Fixed point (FP) technique, which is based on a decomposition of the magnetization characteristic into a linear part (coefficient ν_{FP}) and a residual term ($\boldsymbol{r}$) to be iteratively evaluated. Despite the FP technique requires a higher number of iterations with respect to the most popular Newton–Raphson scheme, it is found to be more efficient, since it does not require the upgrade of the stiffness

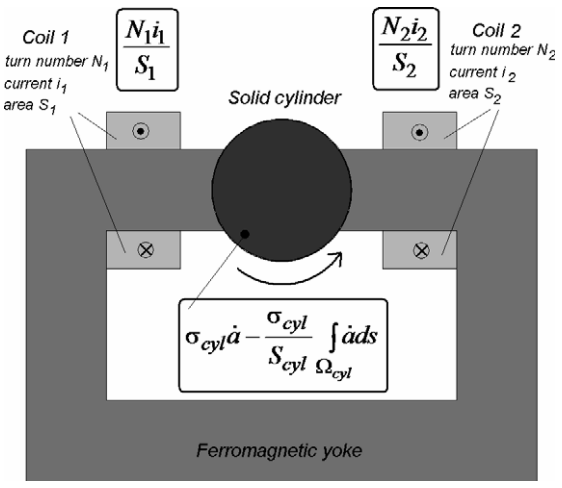

Fig. 1. Scheme of the domain under analysis with the terms of current density appearing in Eq. (2).

matrix at each step. In our application, this feature is even more exploited by adopting a LU factorisation of the system matrix, following the Tinney algorithm [12]; this means that each iteration requires just the solution of two triangular systems. Finally, FP is generally found more accurate in regions with high magnetic saturation levels [13].

The residual term accounts for the non-linearity and it is updated at the generic iteration m, as

$$\boldsymbol{r}_{(m)} = \zeta(\boldsymbol{b}_{(m)}) - \nu_{\mathrm{FP}}\boldsymbol{b}_{(m)}, \tag{3}$$

where $\boldsymbol{r} = (r_x(x,y),\, r_y(x,y), 0)$.

In order to guarantee a convergent scheme, function ζ has to satisfy particular conditions: strong monotony and uniform Lipschitz continuity [14]. Moreover the constant coefficient ν_{FP} has to belong to an interval around the average between the major and the minor rates of curve ζ. Under these hypotheses, the method converges to the solution, whatever the initial value assigned to the residual term.

If ferromagnetic materials show a non-negligible hysteretic behaviour the $\boldsymbol{b}$–$\boldsymbol{h}$ relationship is not a single valued function and a given $(\boldsymbol{b},\boldsymbol{h})$ state depends on the previous magnetic history. In this case the FP iterative scheme requires the use of a hysteresis model able to provide the magnetic field strength evolution starting from the knowledge of the magnetic flux density waveform (inverse hysteresis model). To do this, a model based on the so-called stop hysterons [15,16], specifically tailored for a magnetic vector potential formulation, can be used. As an alternative, Preisach-like models can be adopted employing a modified FP scheme (H-version) [17]. Following this last procedure, at each iteration step, an estimation of the magnetic field strength is obtained as:

$$\tilde{\boldsymbol{h}}_{(m)} = \nu_{\mathrm{FP}}\boldsymbol{b}_{(m)} + \boldsymbol{r}_{(m-1)},$$

then $\tilde{\boldsymbol{h}}$ is used as input for the direct hysteresis model and the new residual value is computed as

$$\boldsymbol{r}_{(m)} = \tilde{\boldsymbol{h}}_{(m)} - \nu_{\mathrm{FP}}\zeta^{-1}\big(\tilde{\boldsymbol{h}}_{(m)}\big).$$

Applying the FP technique and considering expression (2), the resultant field equation, written in the weak form, becomes

$$\int_{\Omega^F} \nu \mathrm{curl}\,\boldsymbol{a}_{(m)} \cdot \mathrm{curl}\,\boldsymbol{w}\,\mathrm{d}s = -\int_{\Omega^F} r_{(m-1)} \cdot \mathrm{curl}\,\boldsymbol{w}\,\mathrm{d}s + \sum_k \left[\sigma_k \int_{\Omega_k} M_{\Omega_k}(\dot{a}_{(m)})\, w\,\mathrm{d}s - \sigma_k \int_{\Omega_k} \dot{a}_{(m)}\, w\,\mathrm{d}s\right] + \sum_p \left[\int_{\Omega_p} \frac{N_p i_p}{S_p}\, w\,\mathrm{d}s\right], \tag{4}$$

where ν is the local value of the magnetic reductivity ($\nu = \nu_{\mathrm{FP}}$ for non-linear media), w is the test function, Ω^F is the entire finite element domain and $M_{\Omega_k}(\dot{a})$ is the mean of $\dot{a}$ over Ω_k. Homogenous Dirichlet boundary conditions complete the electromagnetic field problem. Eq. (4) is discretized using the standard nodal FE technique, with triangular elements and first-order shape functions. In presence of material discontinuities with corners, errors can arise in the solution derivatives, as stated in [18]. Anyway, this problem can be satisfactorily overcome by adopting a suitable fine mesh in the corner regions, which allows the achievement of the requested precision [19].

In voltage driven problems, all or some supply currents i_p appearing in (4) are unknowns and they have to be determined by the interaction with the circuit equations. In this case, it is necessary to add the electric network equations and to introduce relationships linking the circuit and the field quantities. The present paper proposes an approach which combines the integro-differential FE formulation of the transient electromagnetic problem with the conventional Loop current method of the circuit theory.

The external circuit is described in terms of branches. Each of them can be constituted of different electrical components (voltage generators, induced electromotive forces, resistors, inductors) series connected. Thus the branch voltage drop is given by

$$u_{\mathrm{branch}} = Ri + L\frac{\mathrm{d}i}{\mathrm{d}t} + e_p - u_0. \tag{5}$$

The voltage of the generator u_0 represents the known electric source. The induced electromotive force e_p (relative to the generic winding p) introduces the field unknowns in the circuit equations, being expressed as a function of the magnetic vector potential, by the relationship

$$e_p(t) = D\left[\frac{N_p^+}{S_p^+}\int_{\Omega_p^+}\dot{a}\,\mathrm{d}s - \frac{N_p^-}{S_p^-}\int_{\Omega_p^-}\dot{a}\,\mathrm{d}s\right], \tag{6}$$

where D is the domain depth along the z-direction and the integration is performed on the positive (Ω_p^+) and the negative (Ω_p^-) traces of the winding, having respectively cross-sectional area S_p^+ and S_p^- and turn number N_p^+ and N_p^-.

2.2. Mechanical equations and rotation handling

Since the studied electromechanical problem involves moving components, a complete time-domain modelling requires the coupling between the field-circuit equations and the mechanical ones. As the motion law involves the electromagnetic torque acting on the rotor, it is necessary to know its value in order to obtain the solution of the mechanical system. This quantity can be evaluated by the virtual work principle or by the Maxwell Stress Tensor method, that provide the global torques exerted on rigid movable parts.

In this paper, the electromagnetic torque acting on the rotor is computed by the Maxwell stress tensor method. Following this approach, in a 2-D problem, the overall torque is estimated by the numerical integration of the local stress along a closed contour surrounding the rotor and contained in the airgap. In particular, the electromagnetic torque T_{em} can easily be calculated through the relationship

$$\boldsymbol{T}_{\mathrm{em}} = D\int_C \boldsymbol{r}_l \times \left[\frac{1}{\mu_0} b_n b_t \boldsymbol{t} + \frac{1}{2\mu_0}\left(b_n^2 - b_t^2\right)\boldsymbol{n}\right]\mathrm{d}l, \tag{7}$$

where C is any closed line (with tangential unit vector $\boldsymbol{t}$) surrounding the rotor in a region free of sources and magnetic materials, $\boldsymbol{n}$ is the unit outward vector normal to C, b_n and b_t are the normal and tangential components of the magnetic flux density, and μ_0 is the magnetic permeability of air. Vector $\boldsymbol{r}_l$ corresponds to the lever arm (the vector which connects the rotation centre to the midpoint of segment dl). Then, the calculated electromagnetic torque T_{em} is inserted into the mechanical equation

$$J\frac{\mathrm{d}^2\alpha}{\mathrm{d}t^2} = T_{\mathrm{em}} - T_r, \tag{8}$$

where α is the angular position of the moving object, J is the inertial moment and T_r is an applied opposing torque, assumed equal to zero in the following analysis. The time integration of Eq. (8) allows the computation of the rotor angular displacement during a given time interval.

The presence of rotating parts is handled dividing the domain under study into two FE separate meshes: a moving one including the rotor and a portion of air-gap (*master mesh*), and a stationary one containing the remaining fixed domain (*slave mesh*). The two grids are connected through an interface circumference, where the imposition of the magnetic vector potential continuity guarantees the coupling of the two derived sets of equations. For each configuration, a specific algorithm couples the *master nodes*, sliding on the interface, with the *slave* ones, locally adapting the *slave grid*. In particular, the *slave elements* facing the circumference can be subdivided into more triangles, in order to link interface *master nodes* to stationary ones (see Fig. 2). When *slave nodes* on the interface have an intermediate position between two moving ones, they are treated as non-conformal nodes. In other words, the associated magnetic vector potential is expressed interpolating the values of the two nearest conformal nodes belonging to the *master grid* boundary. The weights employed in the linear combination depend on the relative distances from the considered moving nodes.

2.3. Step-by-step procedure

By assembling the FE electromagnetic field problem, described by Eq. (4), and the external circuit behaviour, the following system of ordinary differential equations has to be solved:

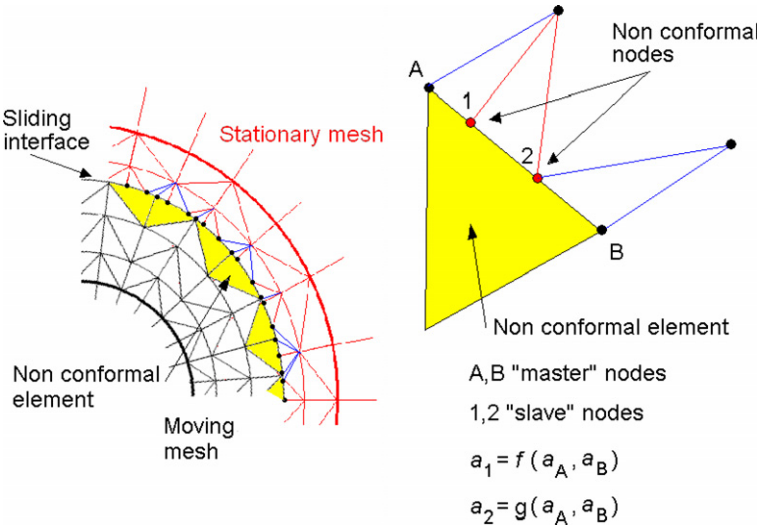

Fig. 2. Moving and stationary meshes and handling of non-conformal nodes. Symbol a represents the nodal value of magnetic vector potential in points 1, 2, A and B.

$$\begin{cases} B_{NN}(\dot{x}) = -[A_{NN}](x) - [A_{NM_1}](y_1) - [A_{NM_2}](y_2) + (c_N) \\ 0 = -[A_{MN}](x) - [A_{MM_1}](y_1) - [A_{MM_2}](y_2) + (c_M). \end{cases} \tag{9}$$

In Eq. (9) matrix A includes the FE stiffness matrix and the circuit terms which do not involve time derivatives; matrix B takes into account the electromagnetic induction phenomena in the field-circuit equations. The right-hand side (c) can be separated into two time dependent vectors (s) and (f) expressing respectively the known sources and the FP residuals.

The problem unknowns are divided into N state variables x (with time derivatives $\dot{x}$) and M algebraic variables y; the algebraic variables are separated into M_1 variables on the interface strips and M_2 ones elsewhere, so that matrix A results to be decomposed into six sub-matrices. This separation is advantageous, because the discretization imposed by the sliding mesh technique causes, at each time step, a variation in the contributions to the system matrix only for the M_1 nodes belonging to the interface strips.

In conclusion, vector (x) state variables of the field-circuit equations, which are:

- the nodal values of the magnetic vector potential in correspondence of materials having an electrical conductivity different from zero (eddy current effect);
- the nodal values of the magnetic vector potential in correspondence of materials electrically connected to the external supply circuit (phenomena of electromagnetic induction);
- the inductive loop currents.

Vector (y) includes the other variables, i.e.:

- the nodal values of the magnetic vector potential in correspondence of materials having an electrical conductivity equal to zero or not connected to the external network;
- the loop currents that involve only resistive components.

The transient analysis is performed by the application of a step-by-step time procedure. In this work we employ the θ-method, that approximates the time derivative of the unknown x in the interval from t to $(t + h)$ by the derivative at a generic instant $(t + \theta h)$, defined by the dimensionless parameter θ $(0 < \theta < 1)$. The recurrence relation, which links the unknown values at two successive time instants (one-step method), is obtained taking into account the following relationships:

$$\dot{x}|_{t+\theta h} \cong (1-\theta)\dot{x}|_t + \theta \dot{x}|_{t+h}, \tag{10}$$

$$\dot{x}|_{t+\theta h} \cong \frac{x|_{t+h} - x|_t}{h}. \tag{11}$$

In accordance with the technical literature, parameter θ is assumed to be greater than 0.5, in order to guarantee the stability of the unknown evolution.

Taking into account that matrix B_{NN} is invariable in time and applying relationships (10) and (11) to system (9), the following algebraic system of equations, at the generic time instant i, is obtained:

$$\begin{cases} B_{NN}(x^i) + \theta h\left[A_{NN}(x^i) + A^i_{NM_1}(y^i_1) + A_{NM_2}(y^i_2)\right] = \theta h(c^i_N) + (p^{i-1}_N) \\ A_{MN}(x^i) + A^i_{MM_1}(y^i_1) + A_{MM_2}(y^i_2) = (c^i_M). \end{cases} \tag{12}$$

The vector (p^{i-1}_N), involving the field-circuit behaviour at the previous instant, is computed for instant t_{i-1}, before the discretization imposed by the rotor displacement, through the recursive form

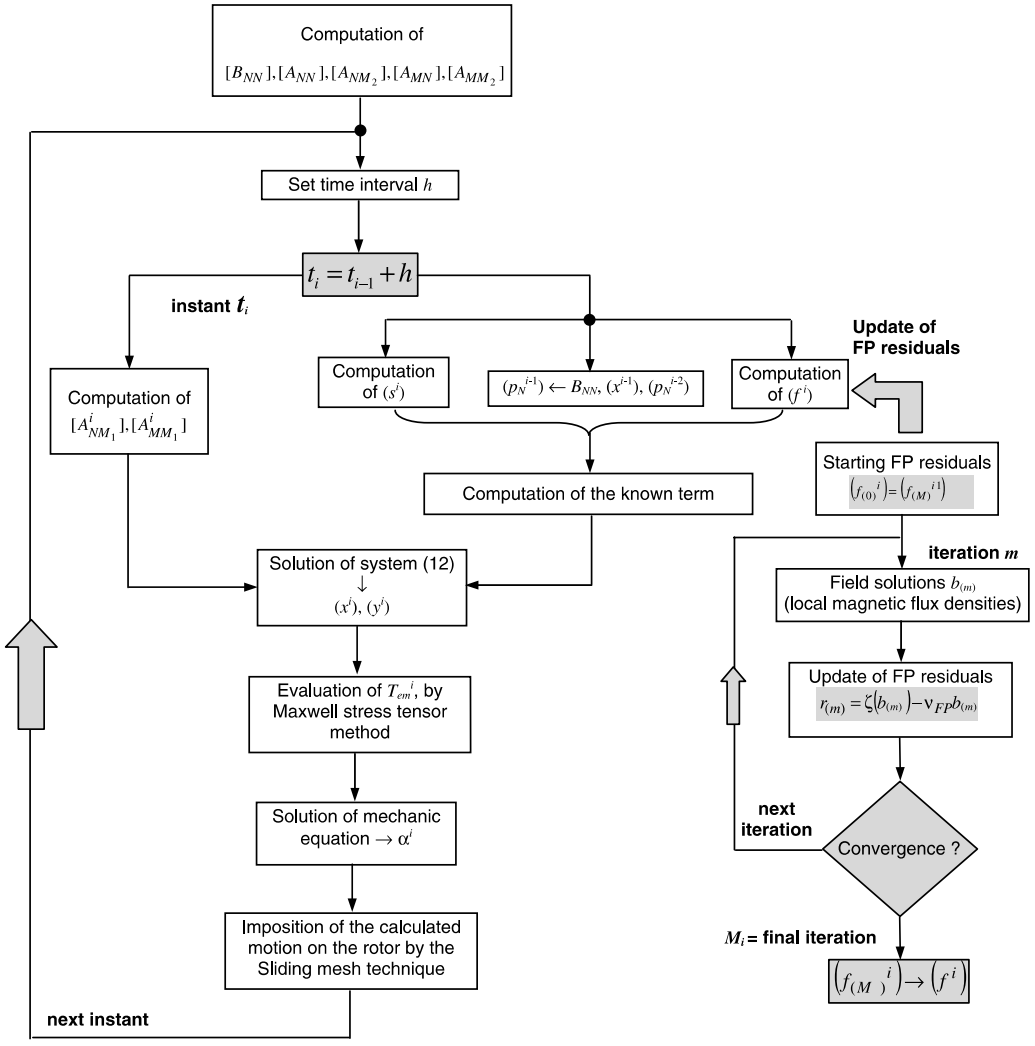

Fig. 3. Flow chart for the computation of the transient evolution of the electromechanical problem and for the update of FP residuals at generic time instant t_i.

$$(p_N^{i-1}) = \frac{1}{\theta} B_{NN}(x^{i-1}) - \frac{1-\theta}{\theta}(p_N^{i-2}), \tag{13}$$

with $(p_N^0) = B_{NN}[(x^0) + (1-\theta)h(\dot{x}^0)]$, allowing the starting from a non-zero stationary case.

The linearized problem (12) is included in the FP scheme, so that at each FP iteration the residual values are updated following relation (3), after the solution of the algebraic system. The iterative procedure takes advantage of the use of residual values computed at the previous instant as starting values for the present time instant (see Fig. 3).

Once the solution of the electromagnetic field problem (12) is obtained at a given instant, the electromagnetic torque is computed by the Maxwell stress tensor method. Then, the application of the step-by-step procedure to Eq. (8), assuming T_{em} constant during the considered time interval, allows the evaluation of the rotor angular displacement and the consequent mesh adapting for the solution of the electromagnetic field problem at the next time instant.

3. Application of the model

The model is applied to the analysis of the electromechanical system shown in Fig. 4a, with the aim of investigating the influence on the mechanical behavior of the material, geometrical and supply parameters. A pure conductive or ferromagnetic cylinder (diameter equal to 150 mm) is disposed among the poles of the magnetic circuit. The cylinder, friction-less and without driving torque, is rotating at the angular speed $\omega_0 = 524$ rad/s (5000 rpm). The supply network of the exciting windings includes a resistance and a voltage generator; the circuit parameters are varied when passing from the analysis of conductive rotors to the study of ferromagnetic ones, in order to generate approximately a comparable magnetic flux in the fixed core. For the sake of comparison, the rotor inertial moment ($J = 0.35 \times 10^{-3}$ kg m^2) is assumed to be the same in all the studied configurations, under the hypothesis that the prevalent contribution is due to the external mechanical load. The finite element model employs ~30 000 elements with ~15 000 nodal unknowns; the time step is of the order of some tens of microseconds, with the time-stepping parameter θ equal to 0.7. In presence of non-linear magnetic behavior the number of FP iterations is of the order of few hundreds at each time instant.

When the device exciting coil is closed on the voltage generator (at $t = 0$), the magnetic field, generated by the supply current, starts to penetrate inside the rotor, impeded by eddy currents which arise together with the field itself, as reported in Fig. 4 for a pure conductive cylinder. These electromagnetic phenomena concur to produce an antagonist torque that tends to slow up the rotor motion. Following the electrical machine theory, the presence of the braking torque can be better explained considering the interaction of two magnetic fluxes. The first one Φ_s, produced by the exciting windings, is directed along x-axis. The second one Φ_r is generated by the eddy currents flowing within the cylinder and it has both x and y components. The braking torque depends on the amplitude of both the fluxes and, in addition, on the value of $\sin\theta$, being θ the spatial angle between Φ_s

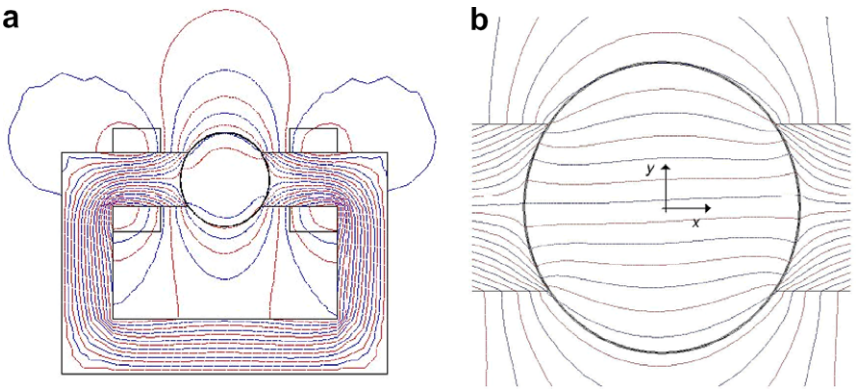

Fig. 4. Electromechanical system under analysis. The flux line distribution in the case of a pure conductive cylinder are represented at the beginning (a) and at the end (b) of the transient evolution.

and Φ_r; thus practically the resulting torque is determined by the y-component of Φ_r. The study of the involved phenomena is further complicated by the fact that, differently from electrical machines, the rotor currents are not localized in the conductors, but distributed over the entire cylinder. All these aspects contribute to make very difficult a a-priori estimation of the influence of the constitutive and geometrical parameters.

3.1. Pure conductive cylinder

A pure conductive solid cylinder is analyzed varying the value of the rotor electrical conductivity σ in a range from 0.1 MS/m to 20 MS/m. Under a d.c. supply voltage, the supply current shows an asymptotic monotonic behavior, following approximately an exponential law. The computed evolution of the cylinder angular speed ω, reported in Fig. 5, evidences how the braking action is not a monotonic function of σ. This behavior is caused by the simultaneous development of different antagonistic phenomena. In fact, the increment of the electrical conductivity gives rise to:

- a tendency to an increase of the induced eddy currents flowing in the rotor;
- a more pronounced skin effect which confines both the magnetic flux density and the current density toward the cylinder periphery (see Fig. 6);
- a reduction of the magnetic flux produced by the windings (see Fig. 7).

These effects cause a variation in the amplitude of Φ_r and in its spatial angle with respect to Φ_s axis, in a way which is not monotonic with the electrical conductivity. This phenomenon is well illustrated in Fig. 8, which presents the y-component of the magnetic flux Φ_r, produced by eddy currents and directly responsible for the braking action: its amplitude increases at the increment of σ up to ~2 MS/m, but sensibly decreases for higher conductivity values.

During the braking action, a portion of the rotor kinetic energy is thermally dissipated by Joule effect, causing an increase of the material temperature. These Joule losses can be estimated from the knowledge of the time-spatial distribution of eddy currents inside the conductive cylinder. The time evolution of the Joule energy, computed for the considered values of the electrical conductivity, is reported in Fig. 9. As expected, the greatest amount of energy is dissipated for the conductivity value of 2 MS/m, which provides the most efficient braking action.

Finally, in order to put in evidence the importance of the flux penetration phenomenon, the analysis is also performed considering a hollow cylinder. Assuming the same operating conditions and an electrical conductivity equal to 2 MS/m, the internal diameter has been varied up to 140 mm. The influence of the hole dimension on the total braking time is summarized in Table 1. The braking time remains unchanged up to internal diameters of 100 mm, showing that the inner part of the cylinder is scarcely interested by the magnetic flux. An

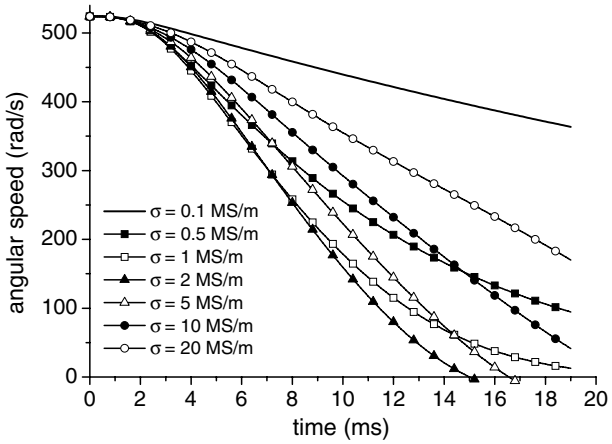

Fig. 5. Evolution of the angular speed for a pure conductive cylinder having different conductivity values.

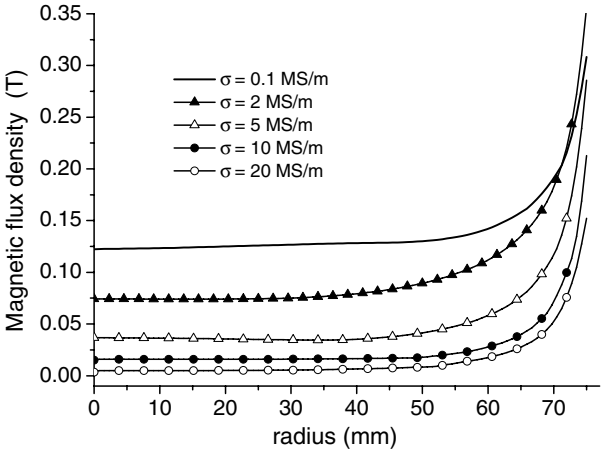

Fig. 6. Distribution of magnetic flux density (peak value) along the cylinder radius for a pure conductive cylinder having different conductivity values.

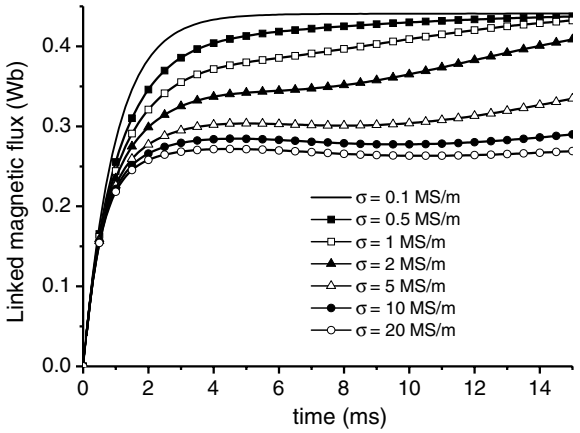

Fig. 7. Evolution of the magnetic flux linked with the supply windings for a pure conductive cylinder having different conductivity values.

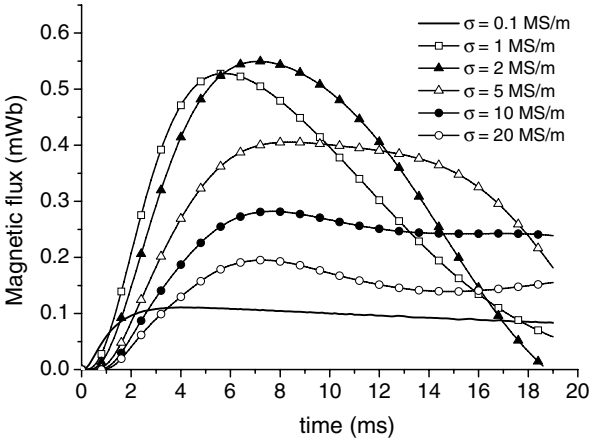

Fig. 8. Time evolution of the y-component of the magnetic flux Φ_r for a pure conductive cylinder having different conductivity values.

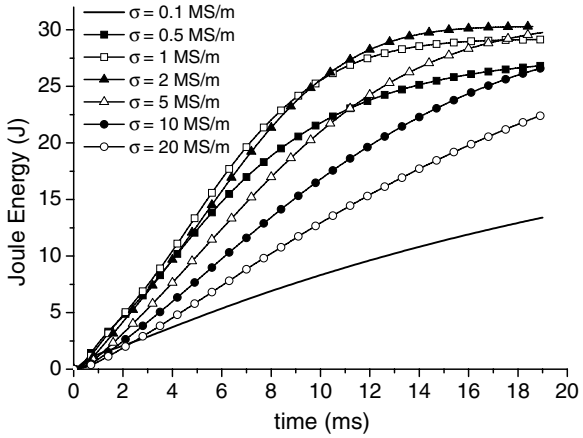

Fig. 9. Evolution of the Joule energy for a pure conductive cylinder having different conductivity values.

Table 1
Braking time for hollow pure conductive cylinders

Internal diameter (mm)	Braking time (ms)
$\leqslant$100	15
120	18
140	60

increase of the braking time occurs only when a portion of material close to the rotor periphery (where the magnetic flux and the current density are concentrated) is removed.

3.2. Ferromagnetic cylinder

The simulation of a ferromagnetic cylinder is performed keeping approximately the same magnetic flux in the fixed core. For such a purpose, the required steady state magnetomotive force has been reduced with respect to the case of a pure conductive cylinder, modifying the supply circuit characteristics. The analysis is initially performed neglecting hysteresis and considering a ferromagnetic material, whose first magnetization curve is reported in Fig. 10.

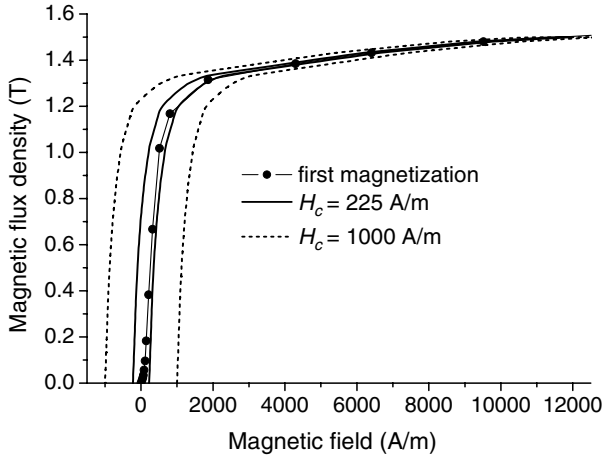

Fig. 10. First magnetization curve and hysteresis loops of the considered ferromagnetic material.

The time evolution of the angular speed and of the Joule energy dissipated in the rotor are plotted in Figs. 11 and 12. Also in this case a non-monotonic behavior versus electrical conductivity is found. The diffusion phenomenon inside the rotor is more pronounced for ferromagnetic with respect to pure conductive materials, as can be observed in Fig. 13a, which reports the instantaneous radial distributions of the induced current density amplitude for $\sigma = 0.1$ MS/m. The corresponding instantaneous magnetic flux lines are presented in Fig. 13b and c for two successive instants.

The transient evolution of the magnetic flux density amplitude, in a point at the rotor periphery, evidences the presence of saturation and a gradual reduction of the number of waveform oscillations, with a corresponding increase of the time period, depending on the braking efficiency (see Fig. 14).

The braking action is also affected by the magnetic hysteresis representing an additional cause of losses that contributes to the dissipation of the kinetic energy stored in the rotating system. To investigate these phenomena, the hysteresis loop of the previous material and one enlarged cycle, having the same magnetization at saturation, but an increased coercive field H_c, are considered (see Fig. 10). The relative evolutions of the angular speed are presented in Fig. 15, for $\sigma = 0.01$ MS/m. As expected, an increase of H_c improves the braking efficiency; however it is generally found that the influence of hysteresis becomes negligible at the increase of the electrical conductivity.

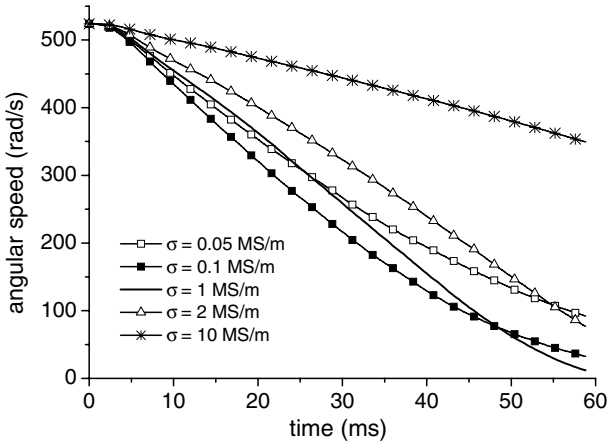

Fig. 11. Evolution of the angular speed for a ferromagnetic cylinder having different conductivity values.

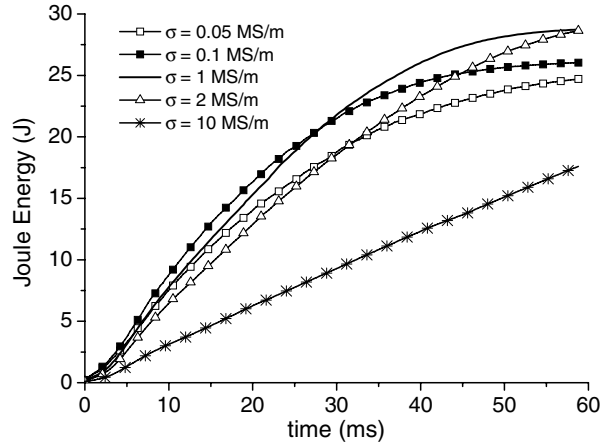

Fig. 12. Evolution of the Joule energy for a ferromagnetic cylinder having different conductivity values.

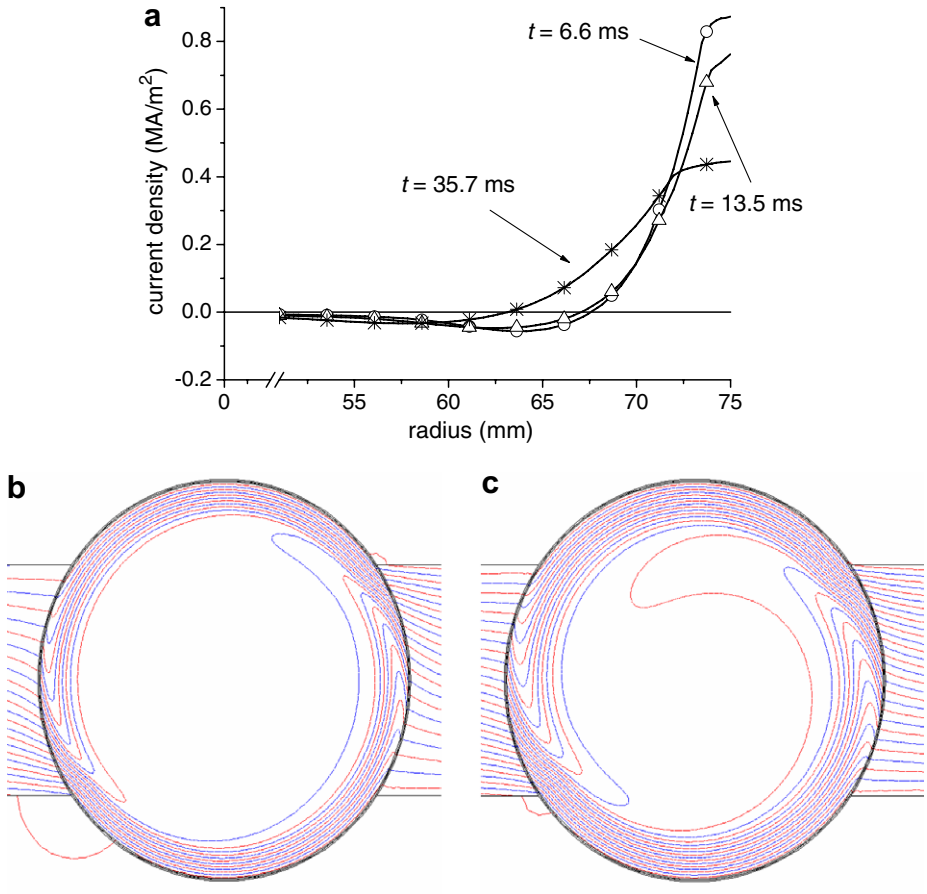

Fig. 13. Diffusion phenomena inside the ferromagnetic cylinder for an electrical conductivity of 0.1 MS/m: (a) radial distribution of current density (instantaneous values); (b) and (c) magnetic flux lines during the transient evolution (time instants equal to 6.6 ms and 35.7 ms respectively).

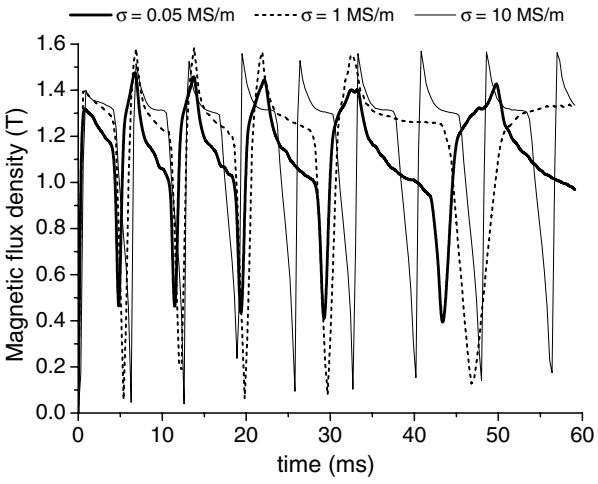

Fig. 14. Transient evolution of the local magnetic flux density amplitude for a ferromagnetic cylinder having different conductivity values. The calculus is made in a point located in the rotor periphery.

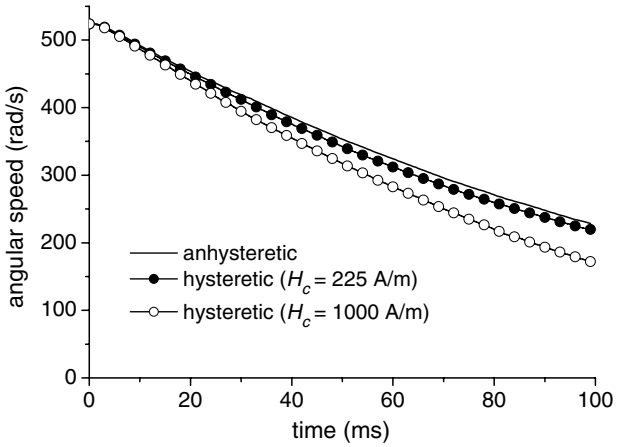

Fig. 15. Evolution of the angular speed for a ferromagnetic cylinder having different hysteresis loops ($\sigma = 0.01$ MS/m).

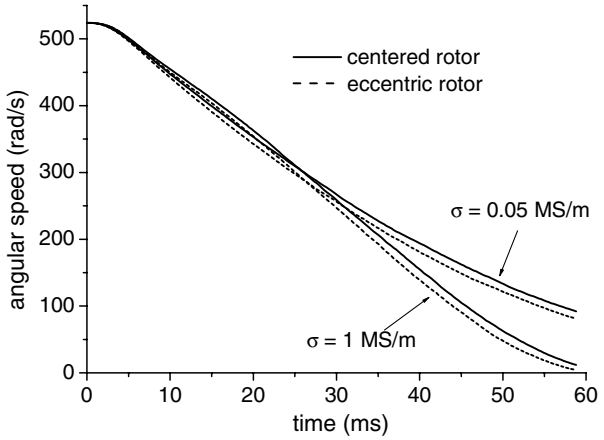

Fig. 16. Evolution of the angular speed for a ferromagnetic cylinder in presence of a static eccentricity.

The presence of a small static eccentricity scarcely influences the electromechanical behavior of the rotor. In the example here analyzed the rotational axis of the cylinder is translated of 0.5 mm (to be compared with an air-gap of 1 mm). This causes a small decrease of the rotor speed only for the ferromagnetic cylinder (see Fig. 16).

Finally, the behavior under 50 Hz supply conditions has been investigated, assuming the r.m.s. value of the supply voltage equal to the d.c. value of the previous analysis. The braking action is significantly reduced, as shown in Fig. 17. The oscillatory evolution of the torque, which also assumes instantaneous positive values due to the delays introduced by eddy currents, directly affects the speed evolution. The influence of the electrical conductivity is also observable; lower values of σ increase the amplitude of the torque oscillations and improve the braking efficiency.

4. Conclusions

In this work a coupled electromagneto-mechanical formulation has been developed and applied to the analysis of a solid cylinder rotating in a magnetic field. Despite the model simplicity, all the physical phenomena governing the device behavior have been taken into account. The results of the analysis, developed under different supply conditions, have put in evidence the fundamental role of the material properties on the braking

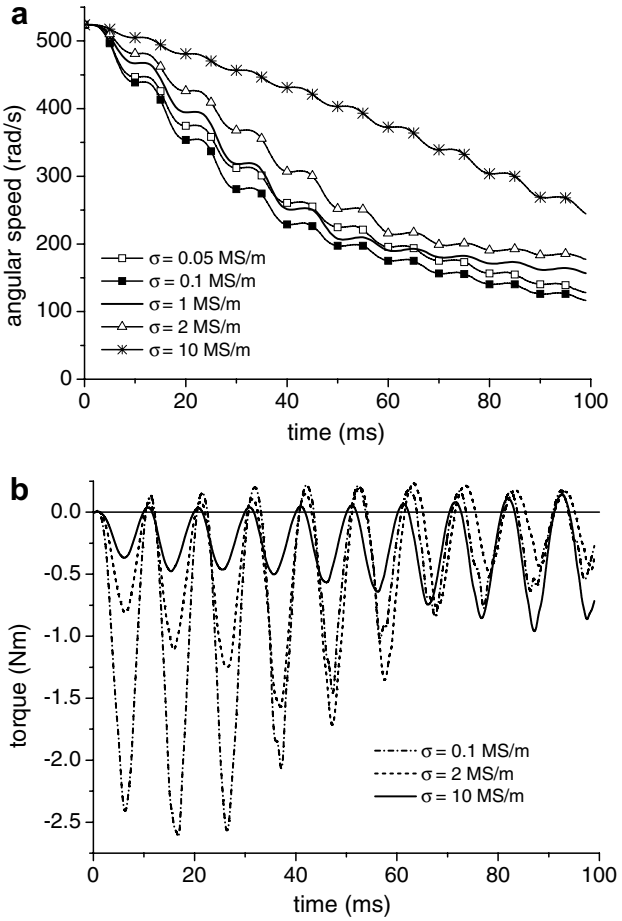

Fig. 17. Evolution of the angular speed (a) and torque (b) for a ferromagnetic cylinder under 50 Hz supply conditions.

action, and consequently the importance of an exhaustive modeling of eddy currents and magnetic saturation phenomena.

References

[1] M.P. Perry, T.B. Jones, Eddy current induction in a solid conducting cylinder with a transverse magnetic field, IEEE Trans. Mag. 14 (1978) 227–232.
[2] T.H. Pham, P.F. Wendling, P. Lombard, S.J. Salon, H. Acikgoz, Dynamic braking of a voltage supplied induction motor using finite element analysis, in: IEEE Electric Machines and Drives Conf. Record (1997) WB3/3.1–WB3/3.3.
[3] M.V.K. Chari, G. Bedrosian, T.J. Sober, J. Scheibel, Two-dimensional time-domain solutions of the eddy current problem in rotating electrical machinery, J. Appl. Phys. 67 (1990) 4714–4716.
[4] S. Niikura, A. Kameari, Analysis of eddy-current and force in conductors with motion, IEEE Trans. Mag. 28 (1992) 1450–1453.
[5] C.R.I. Emson, C.P. Reley, D.A. Walsh, K. Ueda, T. Kumano, Modelling eddy currents induced by rotating systems, IEEE Trans. Mag. 34 (1998) 2593–2596.
[6] H. Kim, C. Lee, Analysis of eddy-currents loss for design of small active magnetic bearings with solid core and rotor, IEEE Trans. Mag. 40 (2004) 3293–3301.
[7] F. Bouillault, A. Buffa, Y. Maday, F. Rapetti, Simulation of a magneto-mechanical damping machine: analysis, discretization, results, Comput. Meth. Appl. Mech. Eng. 191 (2002) 2587–2610.
[8] S. Suuriniemi, K. Forsman, L. Kettunen, J. Mäkinen, Computation of eddy currents coupled with motion, IEEE Trans. Mag. 36 (2000) 1341–1345.
[9] L. Proekt, I.A. Tsukerman, Method of overlapping patches for electromagnetic computation, IEEE Trans. Mag. 38 (2002) 741–744.
[10] H.C. Lai, D. Rodger, Modelling rotor skew in induction machines using 2D and 3D finite element schemes, in: IEEE Electric Machines and Drives Conf. Record (1997) WB3/5.1-WB3/5.3.

[11] A. Buffa, Y. Maday, F. Rapetti, Calculation of eddy currents in moving structures by a sliding mesh – finite element method, IEEE Trans. Mag. 36 (2000) 1356–1359.
[12] E.C. Ogbuobiri, W.F. Tinney, J.W. Walker, Sparsity-directed decomposition for Gaussian elimination on matrices, IEEE Trans. Power App. Syst. 89 (1970) 141–150.
[13] M. Chiampi, D. Chiarabaglio, M. Repetto, An accurate investigation on numerical methods for nonlinear magnetic field problems, J. Magn. Magn. Mat. 133 (1994) 591–595.
[14] M. Chiampi, A. Negro, M. Tartaglia, A finite element method to compute 3-dimensional magnetic field distribution in transformer cores, IEEE Trans. Mag. 16 (1980) 1413–1419.
[15] A.J. Bergqvist, S.A. Lundgren, S.G. Engdahl, Computationally efficient vector hysteresis model using flux density as known variable, in: V. Kose, J. Sievert (Eds.), Non-Linear Electromagnetic Systems, IOS Press, Amsterdam, 1998, pp. 463–466.
[16] O. Bottauscio, M. Chiampi, A. Manzin, Advanced model for dynamic analysis of electromechanical devices, IEEE Trans. Mag. 41 (2005) 36–46.
[17] I.F. Hantila, A method for solving stationary magnetic field in non-linear media, Rev. Roum. Sci. Techn. – Electrotechn. et Energ. 20 (1975) 397.
[18] I. Babuska, Error-bounds for finite element method, Numer. Math. 16 (1971) 322–333.
[19] S. Biddlecombe, J. Simkin, C.W. Trowbridge, Error analysis in finite element models of electromagnetic fields, IEEE Trans. Mag. 22 (1986) 811–813.